CHAPTER 13
SEA CLUTTER

Lewis B. Wetzel
Naval Research Laboratory

13.1 INTRODUCTION

For an operational radar, backscatter of the transmitted signal by elements of the sea surface often places severe limits on the detectability of returns from ships, aircraft and missiles, navigation buoys, and other targets sharing the radar resolution cell with the sea. These interfering signals are commonly referred to as *sea clutter* or *sea echo*. Since the sea presents a dynamic, endlessly variable face to the radar, an understanding of sea clutter will depend not only on finding suitable models to describe the surface scattering but on knowledge of the complex behavior of the sea as well. Fortunately, a close relationship between radar and oceanography has grown up in the remote-sensing community, leading to the accumulation of a large amount of useful information about scattering from the sea and how this scattering relates to oceanographic variables.

It would seem a simple matter to characterize sea clutter empirically by direct measurement of radar returns for a wide variety of both the radar and environmental parameters that appear to affect it. Parameters relating to the radar or its operating configuration, such as frequency, polarization, cell size, and grazing angle, may be specified by the experimenter, but the environmental parameters are quite another matter—for two reasons. First, it has not always been clear which environmental variables are important. For example, wind speed certainly seems to affect clutter levels, but correlation of clutter with, say, ships' anemometer readings has not been entirely satisfactory. The state of agitation of the surface (*sea state*) appears to have a strong effect, but it is a subjective measure, and its relation to the prevailing local winds is often uncertain. Moreover, it has been found that the temperatures of the air and the sea surface can affect the way in which the measured wind speed is related to the generation of clutter-producing waves, yet the importance of these effects were unappreciated over most of the history of sea clutter measurements; so air and sea temperatures were seldom recorded. Even if the importance of an environmental parameter has been recognized, it is often difficult to measure it with accuracy under real-sea conditions, and there are practical and budgetary limits to obtaining open-ocean measurements in sufficient variety to develop any really meaningful statistical models of

clutter. Little wonder that many aspects of sea clutter remain frustratingly ill defined.

Before the late 1960s, most clutter data was collected in bits and pieces from isolated experiments, often with poor or incomplete ground truth. (For reviews of the older literature see, for example, Long,[1] Skolnik,[2] or Nathanson.[3]) Nevertheless, though much of the earlier clutter data was of limited scientific value, it did disclose some general trends, such as the tendency of clutter signal strength at low to intermediate grazing angles to increase with the grazing angle and with wind (or sea state) and generally to be greater for vertical polarization and in upwind-downwind directions.

It is commonly noted that, when viewed on an A scope, the appearance of sea clutter depends strongly on the size of the resolution cell, or *radar footprint*. For large cells it appears *distributed* in range and may be characterized by a surface-averaged cross section with relatively modest fluctuations about a mean value. As the size of the resolution cell is reduced, clutter takes on the appearance of isolated targetlike, or *discrete*, returns that vary in time. At these higher resolutions, the distributed clutter is often seen to consist of a dense sequence of discrete returns. When the discrete returns stand well out of the background, as they are seen to do for both polarizations but most clearly with horizontal polarization at small grazing angles, they are called *sea spikes* and are a common clutter contaminant in this radar operating regime.

Attempts to provide a theoretical explanation of the observed behavior of clutter signals trace essentially from the work pursued during World War II and described in the well-known MIT Radiation Laboratory book edited by Kerr.[4] Unfortunately, the scattering models developed during this period, along with most of those published over the following decade, failed to account for the behavior of sea backscatter in a very convincing way. In 1956, however, Crombie observed that at high-frequency (HF) wavelengths (tens of meters) scattering appeared to arise from a resonant interaction with sea waves of one-half of the incident wavelength, i.e., to be of the Bragg type.[5] Reinforced by the theoretical implications of various small waveheight approximations and wave tank measurements under idealized conditions, the *Bragg model* was introduced into the microwave regime by many workers in the mid-1960s.[6-8] This produced a revolution in thinking about the origins of sea clutter because it involved the sea wave *spectrum*, thus forging a link between clutter physics and oceanography in what became the field of *radio oceanography*. However, fundamental conceptual problems in applying the Bragg hypothesis in microwave scattering, along with recent questions about the validity of its predictions and the possibility of alternative scattering hypotheses, have reopened inquiry into the physical origins of sea scatter and how best to model it.[9-14] This being the case, speculation about physical models will be kept to a minimum in the sections on the empirical behavior of sea clutter. The problem of modeling sea scatter will be discussed separately in a later section.

13.2 DESCRIPTION OF THE SEA SURFACE

Close observation of the sea surface discloses a variety of features such as wedges, cusps, waves, foam, turbulence, and spray, as well as breaking events of all sizes and masses of falling water. Any or all of these might contribute to the scattering of electromagnetic waves responsible for sea clutter. The basic ocean-

ographic descriptor of the sea surface, however, is the *wave spectrum*, which, while saying little about these features, contains a great deal of information about the sea surface in general and is central to the application of the Bragg scattering hypothesis. In view of the need to understand the sea surface in order to understand sea clutter and the prominence of the Bragg hypothesis in existing clutter models, some tutorial material describing the spectral characterization of the sea surface is included below.

There are basically two types of surface waves, *capillary* and *gravity*, depending on whether surface tension or gravity is the dominant restoring force. The transition between one and the other takes place at a wavelength of about 2 cm; so the smaller capillary waves supply the surface fine structure while gravity waves make up the larger and most visible surface structures. Waves have their origin ultimately in the wind, but this does not mean that the "local" wind is a particularly good indicator of what the wave structure beneath it will be. In order to arouse the surface to its *fully developed* or *equilibrium* state, the wind must blow for a sufficient time (*duration*) over a sufficient distance (*fetch*). That part of the wave structure directly produced by these winds is called *sea*. But waves propagate, so even in the absence of local wind, there can be significant local wave motion due to waves arriving from far away, perhaps from a distant storm. Waves of this type are called *swell*, and since the surface over which the waves travel acts as a low-pass filter, *swell* components often take the form of long-crested low-frequency sinusoids.

The Wave Spectrum. The wave spectrum which provides the primary oceanographic description of the sea surface appears in several forms. If the time history of the surface elevation is monitored at a fixed point, the resulting time series may be processed to provide a *frequency spectrum* $S(f)$ of the surface elevation, where $S(f)df$ is a measure of the *energy* (i.e., square of the waveheight) in the frequency interval between f and $f + df$. Wave spectra have been measured in the open ocean primarily for gravity waves down to wavelengths of about 1 m. Open-ocean measurements of capillary waves are especially difficult to perform.[15]

For a gravity wave, the frequency f and the wavenumber K are related by the dispersion relation

$$f = (\tfrac{1}{2}\pi)(gK)^{\tfrac{1}{2}} \tag{13.1}$$

where g is the acceleration of gravity and $K = 2\pi/\Lambda$, with Λ being the wavelength. Although each individual gravity wave obeys this relation, the waves at a point on the sea surface could come from any direction; so they are characterized by a two-dimensional propagation *vector* with orthogonal components K_x and K_y, where the K to be used in Eq. (13.1) is the magnitude $K = (K_x^2 + K_y^2)^{1/2}$.

The wavenumber spectrum associated with $S(f)$ is a function of the two components of K and is commonly written as $W(K_x, K_y)$. This is called the *directional wave spectrum* and expresses the asymmetries associated with winds, currents, refraction, isolated swell components, etc. For a given source of asymmetry like the wind, various parts of the spectrum will display different directional behaviors. For example, in a fully developed sea, the larger waves will tend to move in the direction of the wind while the smaller waves will be more isotropic. Directional spectra are more difficult to measure and are obtained by a variety of experimental methods, such as an array of wave staffs to measure surface heights over a matrix of points, a multiaxis accelerometer buoy, and stereo photography,

and even by processing radar backscatter signals. However, a frequency spectrum measured at a point can contain no knowledge of wave direction; so a wavenumber spectrum $W(K)$ is often defined in terms of the frequency spectrum $S(f)$ by the relation

$$W(K) = S(f(K))(df/dK) \tag{13.2}$$

with the relation between f and K given by Eq. (13.1). To account for the wind direction, $W(K)$ is sometimes multiplied by an empirical function of K and direction υ relative to the (up)wind direction.

Oceanographers have not always been in complete agreement about the form of the frequency spectrum. Nonequilibrium wave conditions, inadequate sampling times, poor ground truth, etc., can contaminate the data set from which empirical spectra are derived. However, by careful selection of data from many sources, ensuring that only equilibrium (fully developed) sea conditions were represented and the wind was always measured at the same reference height, Pierson and Moskowitz[16] established an empirical spectrum that has proved popular and useful. It has the form

$$S(f) = Af^{-5}e^{-B(f_m/f)^4} \tag{13.3}$$

where g is the acceleration of gravity, and $f_m = g/2\pi U$, corresponding to the frequency of a wave moving with a velocity equal to the wind speed U; A and B are empirical constants. This spectrum is illustrated in Fig. 13.1 for several wind
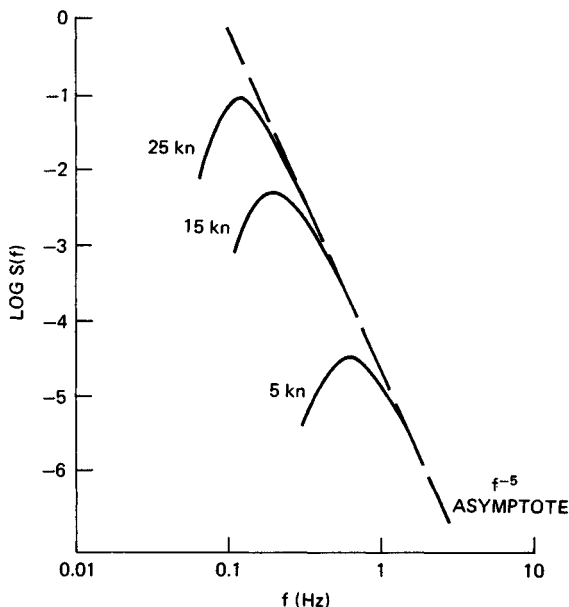

FIG. 13.1 Sea wave frequency spectra of the Pierson-Moskowitz type, representing fully developed seas.

speeds. The effect of increasing wind speed is simply to move the low-frequency cutoff to lower frequencies along the high-frequency f-minus-5 asymptote. (It should be noted that most of the oceanographers' spectra are based on measurements at relatively low frequencies and so cannot be taken seriously at frequencies above about 2 Hz. Nevertheless, these spectral forms are often used up to 20 Hz or greater in predicting radar clutter under the Bragg hypothesis.)

Converting this frequency spectrum into an isotropic wavenumber spectrum through Eq. (13.2) results in a spectrum of similar form, only with a K-minus-4 asymptote. Phillips[17] derived this asymptotic behavior on dimensional grounds, and a widely used simplification, obtained by replacing the smooth peak in Fig. 13.1 by a sharp cutoff, is generally referred to as the *Phillips spectrum* and in wavenumber space is written

$$W(K) = 0.005/K^{-4} \qquad K > g/U^2$$
$$= 0 \qquad K < g/U^2 \qquad (13.4)$$

where the cutoff wavenumber corresponds to the frequency f_m of the peak in Eq. (13.3). Opposed to this highly simplified form are increasingly complex spectra based on more careful empirical studies[18] as well as more sophisticated theoretical considerations.[19,20]

In discussing the characterization of the sea surface by its spectrum, it must be kept in mind that the spectrum is a highly averaged description of how the *energy* of the surface is distributed among the wavenumbers, or frequencies, of the waves present on it. Since the phases of these waves are lost, the spectrum gives no information about the morphology of the surface itself, i.e., about the complex surface features that are responsible for the scattered field. This point will be raised again in the section below on theories of sea clutter.

General Sea Descriptors. The shape of the curves in Fig. 13.1 suggests that the sea wave system has a relatively high Q; so it should be possible to get a rough idea of the behavior of the major waves on the surface by taking the values of *period* ($1/f$) and *wavelength* ($2\pi/K$) defined at the spectral peak. These values belong to a wave satisfying the dispersion relation Eq. (13.1) and having a phase velocity $C = 2\pi \times f/K$ equal to the wind speed U. By using Eq. (13.1), the period T and wavelength Λ thereby defined take the form

$$T = 0.64U \qquad \Lambda = 0.64U^2 \qquad (13.5)$$

where U is in meters per second. Thus, for example, the largest waves in a fully developed sea for a 15-kn (7.5 m/s) wind will have a wavelength of about 120 ft (36 m) with a period of 5 s.

The statistical distribution of waveheights on the ocean surface is quite close to gaussian, with a mean square deviation that can be obtained by integrating the waveheight spectrum over all frequencies (or wavenumbers). For spectra resembling those in Fig. 13.1, the rms waveheight is given approximately by

$$h_{rms} = 0.005U^2 \qquad \text{m} \qquad (13.6)$$

The rms waveheight contains contributions from all the waves on the surface, but very often it is the peak-to-trough height for the higher waves that is of major interest. This is certainly the case for a ship in a seaway or in the shadowing of the surface at low radar grazing angles. The *significant height*, or height of the

one-third highest waves, provides such a measure. It is denoted by $H_{1/3}$ and is taken to be about 3 times the rms height given by Eq. (13.6). For a 15-kn wind, this is only about 3 ft, but for gale-force winds of 40 kn it rises to over 20 ft, which is a rather formidable sea.

Looking at the sea, an observer might describe what he or she sees in terms of a subjective *state of the sea*, e.g., "smooth," "rough," "terrifying!" If these descriptions are listed in order of severity and assigned numbers, these numbers define a *sea state*. A similar numerical scale exists for wind speeds, the *Beaufort wind scale*, with numbers about an integer higher than the corresponding sea state. But it is seldom used in reference to sea clutter.

There are, then, two numbers commonly used to indicate the activity of the sea surface: a subjective sea state and a measured wind speed. Only when the wind has sufficient *fetch* and *duration* to excite a *fully developed* sea, can a wave height be unambiguously associated with it. The surface descriptors generally used in connection with sea clutter—sea state, wind speed, and its associated equilibrium waveheight—are given in Table 13.1, with the wind speed in knots, the significant waveheight in feet, and the duration/fetch required for a fully developed sea in hours/nautical mile. It is of interest to note that the median wind speed over the world's oceans is about 15 kn, corresponding to sea state 3.

TABLE 13.1   Sea-Surface Descriptors

Sea state	Wind speed, kn	Waveheight $H_{1/3}$, ft	Duration/fetch, h/nmi
1 (smooth)	< 7	1	1/20
2 (slight)	7–12	1–3	5/50
3 (moderate)	12–16	3–5	15/100
4 (rough)	16–19	5–8	23/150
5 (very rough)	19–23	8–12	25/200
6 (high)	23–30	12–20	27/300
7 (very high)	30–45	20–40	30/500

13.3 EMPIRICAL BEHAVIOR OF SEA CLUTTER

Sea clutter is a function of many parameters, some of them showing a complicated interdependence; so it is not an easy task to establish its detailed behavior with a great deal of confidence or precision. For example, in a proper sea clutter measurement, the polarization, radar frequency, grazing angle, and resolution cell size will have been specified. Then the wind speed and direction must be measured at a reference altitude, and if the results are to be compared with those of other experimenters, the proper *duration* and *fetch* should be present to ensure standardization to equilibrium sea conditions. Since these measured winds are related to the wind structure at the surface through the atmospheric boundary layer, the shape of this layer must be determined by measuring the air and sea temperatures. To complicate the picture still further, it is becoming increasingly clear that sea backscatter has a strong dependence on the direction of the long waves, which include *swell*, in the measurement area; so ideally the *directional wave spectrum* should be measured as well. Obviously, it is unlikely that all these

environmental parameters will be recorded with precision in every (or even *any*) sea clutter measurement; so considerable variability in the basic conditions under which sea clutter data is collected by different experimenters can be expected. It is of interest to note that in many of the reported measurements of sea clutter, particularly in the older literature, wide inconsistencies between wind speed and waveheight may be found. For example, a wind speed of 5 kn might be reported with waveheights of 6 ft, or 20-kn winds with 2-ft waves. These pairings are inconsistent with the values for an equilibrium sea described in Table 13.1 and indicate the unnoticed presence of heavy swell or highly nonequilibrium wind conditions, or both. Even with all the variables properly specified, recorded clutter data can be spread over a wide dynamic range, often as great as 40 dB at low grazing angles, so that clutter behavior is best described in terms of probability distribution functions.

Since sea clutter is generally viewed as a surface-distributed process, the basic clutter parameter is taken to be the normalized radar cross section (NRCS), σ^0, of the surface, commonly referred to as *sigma zero* and expressed in decibels relative to 1 m^2/m^2. It is obtained experimentally by dividing the measured radar cross section of an illuminated patch of the surface by a normalizing area; so differences in the definition of this area can lead to inconsistencies among various reports of NRCS measurements. Scattering from any distributed target involves the product of the transmitting and receiving system footprints integrated over the target. These footprints cover exactly the same area for a monostatic radar and will depend on the pulse and beamwidths, the range, and the grazing angle. If the footprints are assumed to be of the *cookie-cutter* type (constant amplitude falling sharply to zero at the half-power points), then the relation between the actual radar clutter cross section σ_c, as inferred from the received power via the radar equation, and the NRCS σ^0 is given by

$$\sigma^0 = \sigma_c/A_f \tag{13.7}$$

where for a radar with an antenna beamwidth B and rectangular pulse of length T, viewing the surface at range R and grazing angle θ, the area A_f is either

$$A_f = \pi(BR)^2/4\sin\theta \tag{13.8}$$

for beam-limited conditions [e.g., continuous-wave (CW) or long-pulse radar at high grazing angles] or

$$A_f = (c\tau/2)BR/\cos\theta \tag{13.9}$$

for pulse-width-limited conditions (e.g., short-pulse radar at low grazing angles).

Real radars do not produce cookie-cutter footprints, however, since the antenna beam will have, say, a Bessel or gaussian profile and the pulse might be shaped. For this reason, an effective A must be obtained from a surface integration of the square of the actual amplitude profile of the footprint, which will always result in a smaller value of A than that defined by Eq. (13.8) or Eq. (13.9), and therefore in larger values of σ^0 as derived from measured values of σ_c by Eq. (13.7). Most experimenters use the half-power beamwidth in Eq. (13.8) or Eq. (13.9), with an error that is usually only 1 or 2 dB.

Dependence on Wind Speed, Grazing Angle, and Frequency. It was noted earlier that summaries of clutter measurements made before about 1970 may be found in several of the standard reference books on radar[2,3] and radar clutter.[1] Among the programs of this period, the most ambitious was that pursued in the late 1960s at the Naval Research Laboratory (NRL),[21] in which an airborne four-frequency radar (4FR), operating with both horizontal and vertical polarizations at UHF (428 MHz), L band (1228 MHz), C band (4455 MHz), and X band (8910 MHz), made clutter measurements upwind, downwind, and crosswind in winds from 5 to 50 kn for grazing angles between 5 and 90°. The system was calibrated against standard metal spheres, and wind speeds and waveheights were recorded in the measurement areas from instrumented ships.

Typically, samples of σ^0 for a given set of radar and environmental parameters are scattered over a wide range of values and in the NRL experiments were organized into probability distribution functions of the type shown in Fig. 13.2. The
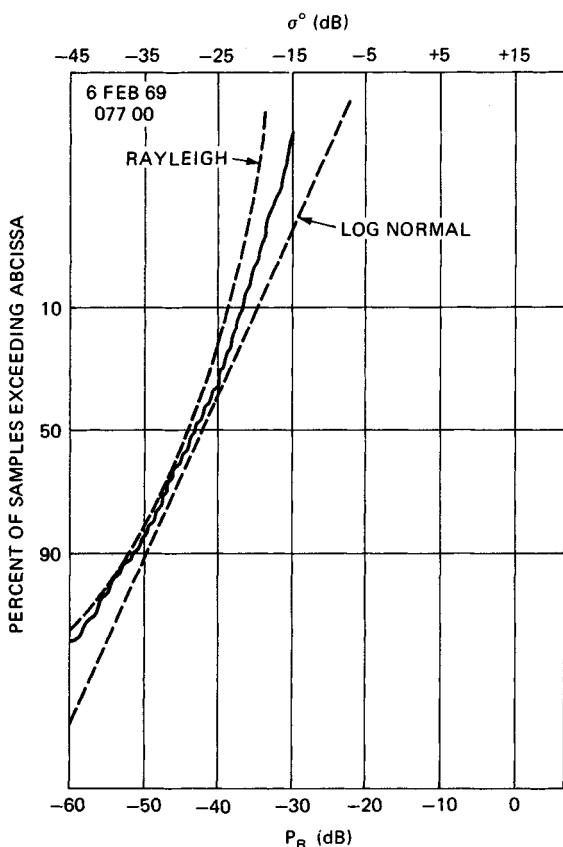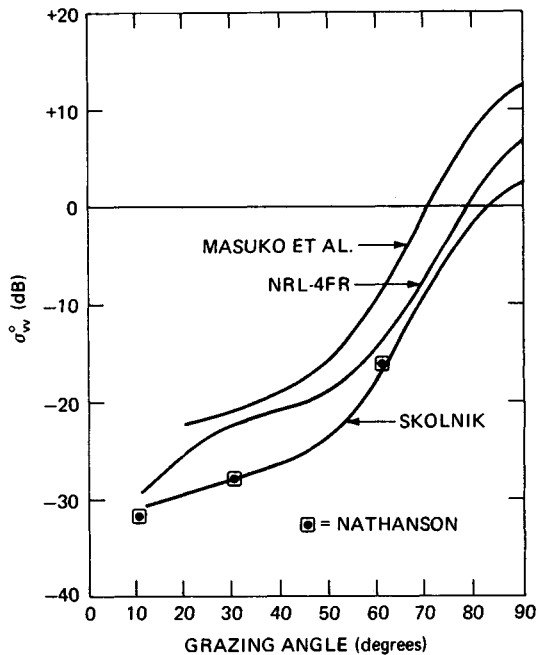

FIG. 13.2 An example of the probability distribution of sea clutter data. (*From Daley.*[21])
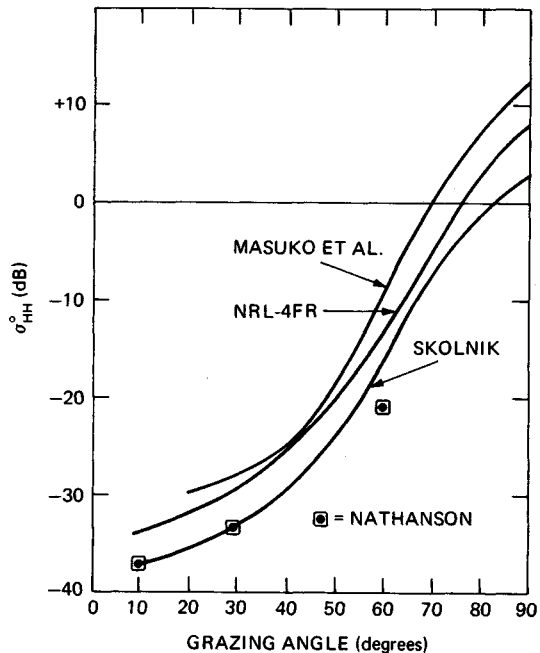
data, represented by the solid line, is plotted on normal probability paper with Rayleigh and log-normal distributions shown for comparison (dashed lines). The ordinate is the *percent of time by which the abscissa is exceeded*, and the abscissa is the value of σ^0 as defined by Eq. (13.7), with A taken from Eq. (13.8) or Eq. (13.9) as appropriate. This particular distribution is representative of clutter from a relatively large radar footprint (pulse length about 0.5 μs) measured at intermediate grazing angles (20 to 70°) for moderate wind speeds (about 15 kn). It is Rayleigh-like but shows a tendency toward log-normal behavior for the larger cross sections. From a detailed statistical analysis of the NRL 4FR data, Valenzuela and Laing[22] concluded that, for this data at least, the distributions of sea clutter cross sections were intermediate between the exponential (which is the power distribution corresponding to Rayleigh-distributed scattered-field amplitudes) and log-normal distributions.

Organizing the data samples into probability distributions makes the *median* (50 percent) value a convenient statistical measure of the clutter cross section. But many investigators process their data to provide the *mean* value, and since the conversion of a *median* to a *mean* requires knowledge of the probability distribution function, care must be taken to avoid ambiguity in comparing the measurements of different experimenters. The original analysis of the NRL 4FR data was based on *median* cross sections and the assumptions of the cookie-cutter antenna beam embodied in Eqs. (13.8) and (13.9).[21,23] In later presentations of this data,[24] the *median* values of σ^0 were replaced by *means*, raising them by about 1.6 dB, and the area A in Eq. (13.7) was redefined in terms of a more realistic tapered footprint, adding another 1 to 2 dB. This means that there is a difference of 3 to 4 dB between the earlier and later presentations of the same data, and since these results are widely used and quoted, it is important to ensure that the proper definition of σ^0 is being used when comparing them with clutter data that has been taken by other experimenters or in using these results in clutter predictions.

General Results. Being the first really comprehensive collection of clutter data over a wide range of radar frequencies, the 4FR program produced many plots showing the dependence of sea clutter on grazing angle, frequency, polarization, wind direction, and wind speed. However, comparison of these plots with others made both earlier and later shows the extent of the variations to be found in sea clutter measurements reported by different investigators for exactly the same set of parameters. This is seen clearly in Fig. 13.3a and b, which compares the grazing-angle dependence of X-band clutter data for wind speeds in the neighborhood of 15 kn obtained from four sources: NRL 4FR[24] (these are *mean* results for upwind directions and include the antenna corrections mentioned above), aircraft measurements by Masuko et al.[29] (also in the upwind direction), and summaries of the older data (pre-1970) taken from books on radar systems by Skolnik[2] and Nathanson.[3] The discrepancies between the different data sets can be accounted for, at least in part, as follows. The older data set was based on published measurements from various sources, and since there is no specification of wind direction, it may be assumed that it represents some kind of average of upwind, downwind, and crosswind directions. As will be seen below, this average is about 2 to 3 dB smaller than the upwind returns. Moreover, the *early* NRL 4FR data was used liberally in the older data summaries, and it was noted above that there is a difference of 3 to 4 dB between the early and later presentations of the same NRL 4FR data, the latter being used in Fig. 13.3a and b. With these

FIG. 13.3 Comparison of X-band clutter data from different sources for a nominal wind speed of 15 kn. (*a*) Vertical polarization. (*b*) Horizontal polarization. (*Based on data from Masuko et al.,*[29] *NRL 4FR,*[21] *Skolnik,*[2] *and Nathanson.*[3])

corrections, the curves would show closer agreement. Nevertheless, it is clear that uncritical use of published clutter data could lead two radar systems designers to choose sea clutter estimates almost an order of magnitude apart for the same conditions.

The NRL 4FR data set is unique in that no other program has reported measurements made over so wide a range of frequencies, grazing angles, and wind speeds at the same time. Figure 13.4 shows the trends for both vertically and horizontally polarized sea clutter over a range of grazing angles down to 5°. The curves represent the centers of ±5 dB bands which contain the major returns for the three higher frequencies (L, C, and X bands—the UHF returns were a few decibels lower) and wind speeds above about 12 kn. The major differences in sea clutter for the two polarizations are seen to lie in the range of grazing angles between about 5 and 60°, where the horizontally polarized returns are smaller. This difference is found to be emphasized at both lower wind speeds and lower frequencies. The cross sections approach each other at high angles (>50°) and, for the higher microwave frequencies, at low angles (<5°) as well. In fact, for grazing angles less than a few degrees and moderate to strong wind speeds, several observers have reported that at X band and at the higher sea states the horizontally polarized returns often exceed the vertically polarized returns.[1,25,26]

The NRL 4FR system permitted transmission and reception on orthogonal polarizations so that data could be collected for cross-polarized sea clutter. These returns tended to have a weak dependence on grazing angle and were always smaller than either of the like-polarized returns, lying in the cross-hatched region shown on Fig. 13.4.

It is informative to compare measurements by different investigators in different parts of the world under similar wind conditions. Figure 13.5 displays measurements of vertically polarized sea clutter down to a grazing angle of 20° for wind speeds of about 15 kn.from three independent experiments using airborne radars at C-, X-, and K-band frequencies.[27–29] While there is no assurance that all these measurements were made over fully developed seas, it is clear that there is a rather strong consistency among them, which reinforces the observation made in reference to Fig. 13.4 that the frequency dependence of sea clutter at intermediate grazing angles is weak at microwave frequencies from L to K band.

Dependence on Wind Speed. The relation between sea clutter and wind speed is complex and uncertain, since it has been found to depend on almost all the parameters that characterize sea clutter: frequency, grazing angle, polarization, the state of the sea surface, the direction and speed of the wind itself, and even on whether the measurements are made from an aircraft or a tower platform.[30]

A common way to organize clutter data is to seek the best straight-line fit (linear regression) between clutter cross sections in decibels and the log of the wind speed (or some other parameter). This, of course, *imposes* a power-law relation between the variables: $\sigma^0 \propto U^n$, where n is determined by the slope of the
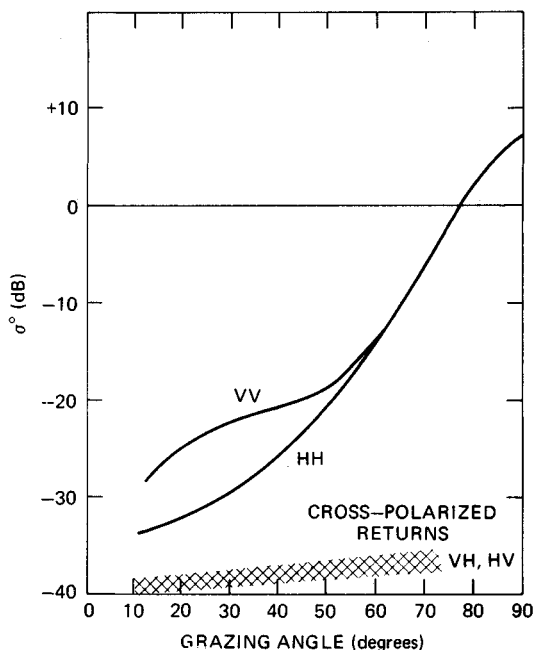
FIG. 13.4 General trends in clutter behavior for average wind speeds (about 15 kn) based on NRL 4FR data. Plots represent L-, C-, and X-band data within ±5 dB.
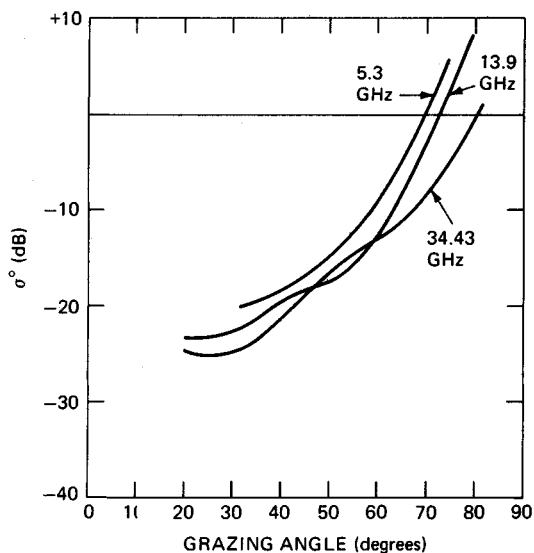

FIG. 13.5 Frequency dependence of sea clutter for wind speeds of about 15 kn: 5.3 GHz, Feindt;[27] 13.9 GHz, Schroeder;[28] 34.4 GHz, Masuko.[29]

line. An example is shown in Fig. 13.6.[31] On the other hand, the totality of the NRL 4FR results appeared to show saturation for wind speeds above about 20 kn, but the high and low- to moderate- wind-speed data was collected at different times in different places under different conditions of sea-surface development, and discrepancies between the two data sets for common wind speeds have weakened the evidence for saturation.[32] Other investigators deny that it is even possible to express wind dependence in the form of a power law, proposing the existence of a kind of threshold wind speed, below which clutter virtually vanishes and above which the clutter level rises toward a saturation value.[18] This is indicated by the curves in Fig. 13.7, where the straight lines correspond to various power laws. Once this possibility is raised, it is possible to find examples of data that appear to track such a curve while at the same time yielding a power law by linear regression, as illustrated in the tower data shown in Fig. 13.8.[31] This behavior is not uncommon.
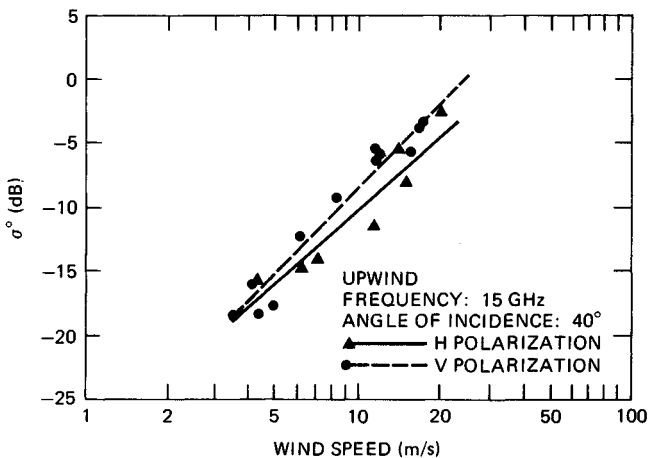

FIG. 13.6   Sea clutter from a tower platform with power-law wind-speed dependence defined by linear regression. (*From Chaudhry and Moore,*[31] © *1984, IEEE.*)

Nevertheless, the imposition of a power-law relation provides a convenient way to visualize trends in the behavior of sea clutter with wind speed. The various aircraft measurements referred to above[27–29] as well as data from a tower in the North Sea[30,31] were all treated in this way, yielding plots of σ^0 as a function of wind speed and grazing angle of the form shown in Fig. 13.9a and b. Plots of this type give information about both the wind-speed and grazing-angle dependence of sea clutter for a given frequency, polarization, and wind direction. Figure 13.9a and b is based on a blend of radiometer-scatterometer (RADSCAT) data at 13.9 GHz[29] and measurements by Masuko et al. at 10 GHz,[29] both for upwind directions. Thus they can be viewed as representative of clutter behavior in the vicinity of X band, since the difference between the two frequencies is small. However, examination of the data points underlying these linear regressions show point scatter that sometimes resembles Fig. 13.6, sometimes Fig. 13.8, and sometimes neither; so the straight lines in these figures cannot be taken too seriously. In fact, it appears that there is no simple functional dependence of
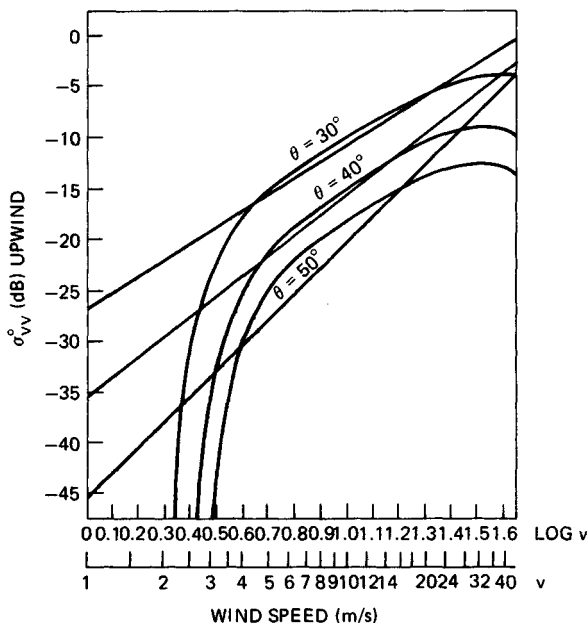
FIG. 13.7 A hypothetical wind-speed dependence of sea clutter (curved traces) compared with various power laws (straight lines). (*Derived from Pierson and Donelan.*[18])
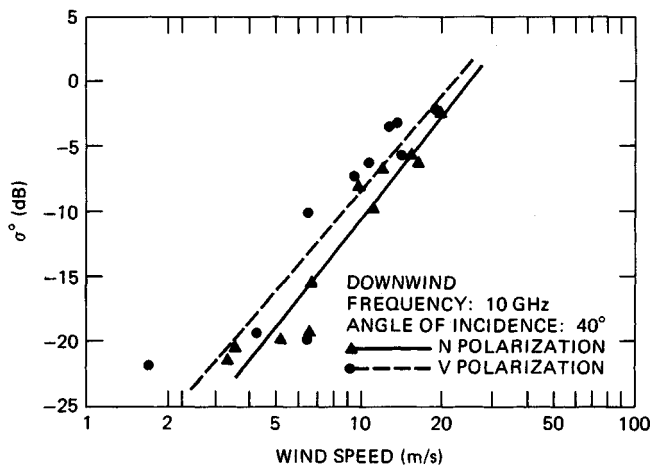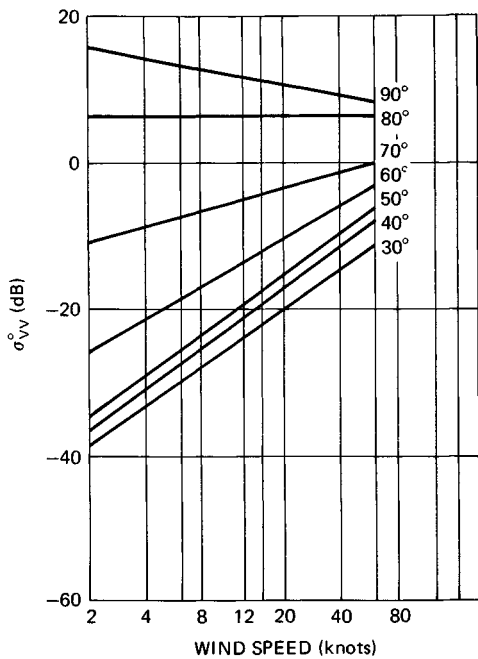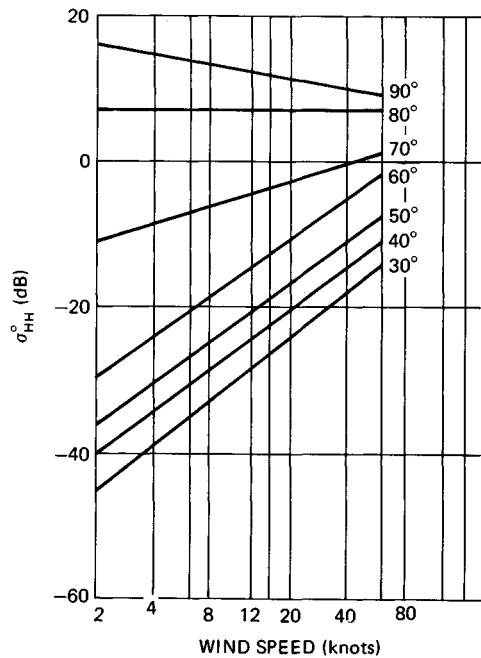

FIG. 13.8 Example of forcing a power-law fit (compare data with curves in Fig. 13.6). (*From Chaudhry and Moore,*[31] © *1984, IEEE.*)

FIG. 13.9 Example of clutter behavior with wind speed and grazing angle—average of data at 10 GHz[29] *and 13.9 GHz.*[28] (*a*) Vertical polarization. (*b*) Horizontal polarization.

sea clutter on wind speed that can be established with any confidence from existing data, although most investigators would probably agree that the behavior of microwave sea clutter with wind speed at intermediate grazing angles can be roughly described as follows: for light winds (less than 6 to 8 kn) sea clutter is weak, variable, and ill defined; for intermediate winds (about 12 to 25 kn) it can be described roughly by a power law of the type found in Fig. 13.6; and for strong winds (above about 30 kn) there is a tendency for it to level off. In fact, the convergence of the lines in Fig. 13.9a and b with increasing wind speed suggests that the reflectivity of the sea surface is tending toward Lambert's law, for which there is no dependence on grazing angle, frequency, or polarization but only on surface *albedo*.

Dependence on Wind Direction.   In several of the experiments referenced above, the dependence of sea backscatter on angle relative to the wind direction was found by recording the radar return from a spot on the surface while flying around it in a circle. Figure 13.10a and b gives an example of this behavior for grazing angles of about 45° and wind speeds close to 15 kn.[29] The figures contain results obtained independently by three different groups. The behavior shown here is representative of that found generally: sea clutter is strongest viewed upwind, weakest viewed crosswind, and of intermediate strength viewed downwind, the total variation being about 5 dB.

At High Grazing Angles.   The top curve in Fig. 13.9a and b corresponds to clutter at a grazing angle of 90°, that is, for a radar looking straight down. On a strictly empirical basis, the clutter cross section at this angle is only weakly de
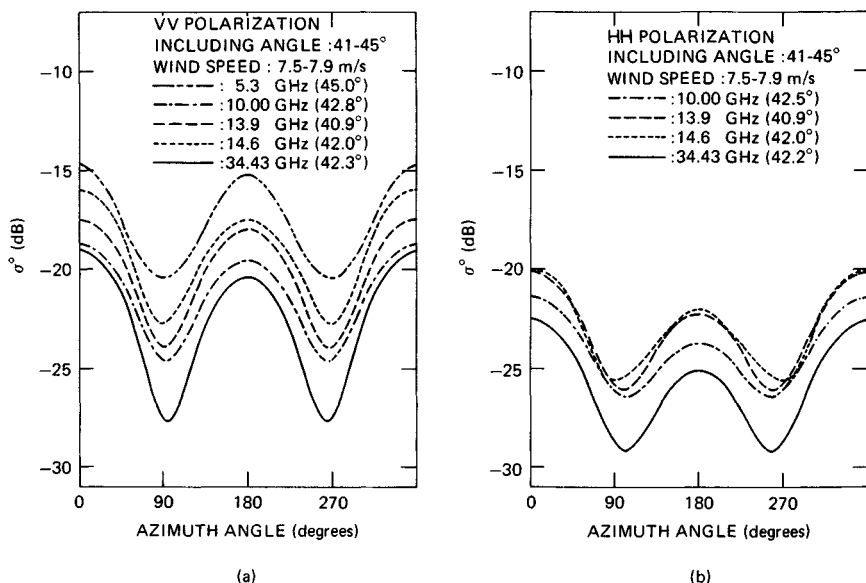

FIG. 13.10   Dependence of clutter on wind direction: nominal wind speed, 15 kn; grazing angle, 45°. (*From Masuko et al.,*[29] © *by the American Geophysical Union.*)

pendent on frequency, has a maximum of about +15 dB at zero wind speed (at least for the antenna beamwidths and experimental configurations reported), and falls off gradually as the wind picks up. Scattering at high grazing angles is commonly regarded as a form of specular scattering from tilted facets of the surface; so it is of interest to note that there appears to be a small range of angles in the neighborhood of 80° for which the cross section is almost completely independent of wind speed. Since these angles correspond to complements of the common rms sea slope angles of about 10°, it might be argued that as the wind increases, the clutter decrease due to increasing surface roughness is balanced at these angles by a clutter increase due to an increasing population of scattering facets. This line may therefore be regarded as the boundary separating the *specular* regime, where the cross section is decreased by surface roughness, from the *rough-surface* regime, where the cross section increases with surface roughness. It should further be noted that clutter measurements at these high grazing angles will be relatively sensitive to the averaging effects of wide antenna beamwidths, which could become a source of ambiguity in aircraft measurements at the lower radar frequencies.

At Low Grazing Angles. At low grazing angles, below mean sea slope angles of about 10°, sea clutter takes on a different character. The sharp clutter peaks known as sea spikes began to appear on A-scope presentations,[1,25,33] and the probability distributions assume a different form.[34] Figure 13.11 shows the presence of sea spikes in the time histories of returns from a fixed spot, measured from a tower in the Gulf of Mexico with a high-resolution X-band radar looking into an active sea at a 1.5° grazing angle.[33] The vertically polarized returns appear to be a bit broader, and while the horizontally polarized returns are more spiky, both polarizations display the sharp bursts characteristic of sea clutter at small grazing angles. The peak cross sections in these records are of the order of 10 m² and are roughly the same for the two polarizations, which is another characteristic of sea clutter at these angles. Interestingly, while the same measurements made in "calm" water looked virtually identical in every detail, peak cross sections were now only 10 cm², or 40 dB, less.
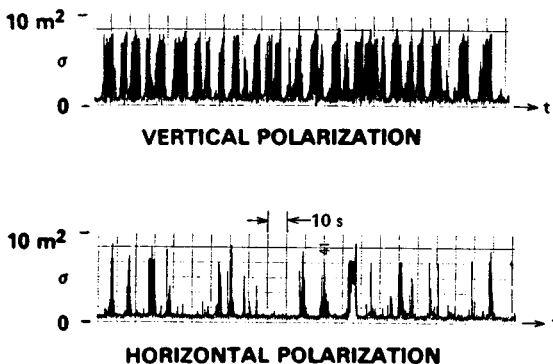

FIG. 13.11   Sea spikes at X band, 1.4° grazing angle, moderate to strong winds. Note equal amplitudes at the two polarizations. (*From Lewis and Olin.*[33])

Trizna has accumulated a considerable body of data from measurements of low-angle sea clutter using high-resolution (40-ns) shipboard radar in both the Atlantic and the Pacific oceans.[34] The probability distributions of the clutter cross sections were plotted in the manner of Fig. 13.12, which shows the distributions of horizontally polarized X-band data at a 3° grazing angle for low, medium, and high wind speeds (in order from left to right). The low-wind trace corresponds to a Rayleigh distribution, while the other straight-line segments are two-parameter Weibull distributions defined by different parameter pairs. It is clear that the behavior is different and considerably more complex than that shown in Fig. 13.2 for the higher grazing angles and wider pulses. Trizna interprets these distributions as follows: in each trace, the left-hand segment (lowest cross section) is actually receiver noise, recorded when the radar footprint lay in shadow; the middle section corresponds to distributed clutter, for reasons relating mainly to its weak dependence on resolution cell size; the right-hand section (highest cross section) describes the sea spikes, for reasons relating to the dependence on wind speed (similar to whitecap dependence) and the sheer size of the components (some individual absolute cross sections in excess of 1000 m^2). For the higher wind speeds and fully developed seas encountered in the North Atlantic, the population of this sea-spike sector (the percentage of sea spikes) was found to grow as the 3.5th power of the wind speed, which, interestingly, is the same wind-speed dependence shown by the percentage of whitecaps seen on the surface.[36]
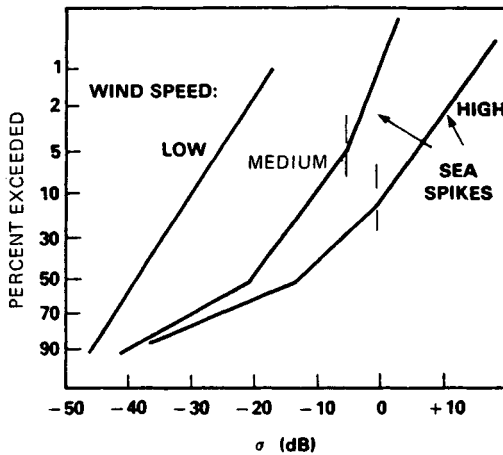

FIG. 13.12 Segmented clutter probability distributions at low grazing angles. (*Based on Trizna.*[34])

It should be kept in mind that, to the extent that the sea surface may be viewed as a stationary homogeneous process, as it generally is over the duration and spatial extent of any particular experimental event, the scattering cross section may be said to be *ergodic*, which means that the statistical results obtained by time averaging from a small cell are equivalent to a shorter time average from a larger cell, provided that the number of "samples" is the same in the two cases. For this reason, the statistical implications of experimental data can be properly compared only if the details of the sampling procedure are specified. However, the number of samples in the experimental results shown thus far have been suf-

ficiently large that the differences between, for example, Figs. 13.2 and 13.12, may be considered real and related to differences in grazing angle rather than in resolution cell size. In fact, distributions closely resembling those in Fig. 13.12 were obtained much earlier from similar measurements with considerably broader pulse widths.[35]

At Very Low Grazing Angles. There is some evidence that sea clutter might drop off more sharply below a *critical angle* in the neighborhood of a degree or so (see Long[1]). This critical angle, or *critical range* for a radar at a fixed height, has been observed from time to time since first noted in early observations of sea clutter.[4] According to Katzin,[37] the critical angle occurs as a result of interference between direct and (perfectly) reflected rays at the scattering *targets* responsible for the clutter signal. While this simple picture can account for the *R*-minus-7 decay sometimes observed, a critical angle often fails to materialize, and when it does, it need not show an *R*-minus-7 decrease with range (or the equivalent fourth-power dependence on grazing angle).[1] An alternative explanation for this behavior, applicable at the higher microwave frequencies, has been suggested by Wetzel,[12,38] based on a *threshold-shadowing* model for upwind and downwind directions that implies a sharp decrease in the average cross section for grazing angles below a few degrees. In crosswind directions, with the radar looking along the troughs of the major waves, a much milder shadowing function will apply; so there should be a clear distinction between the upwind-downwind and crosswind behavior of sea clutter at very low grazing angles.

Examples of clutter behavior at these angles may be found in independent measurements at relatively high wind speeds by Hunter and Senior off the south coast of England[39] and by Sittrop off the west coast of Norway.[40] Their results for orthogonal directions relative to the wind are shown in Fig. 13.13, along with the predictions of a conventional shadowing function[41] and the threshold-shadowing function.[38] It would appear that a combination of conventional shadowing (which goes as the first power of the grazing angle) across the wind and threshold shadowing in upwind and downwind directions accounts for the observed behavior of this very low angle clutter quite well. The decay law for low-angle clutter should therefore depend on the viewing angle relative to the wind direction; so it might occur with powers between the first and the fourth. This is just what is observed.[42] It should be remarked, however, that shadowing at low grazing angles is a complex phenomenon (see below), and the physical origin or even the existence of a critical angle is still open to question. Moreover, there is relatively little good data on very low angle clutter for other than X-band frequencies; so the general behavior of sea clutter in this angular regime remains uncertain.

At HF and Millimeter-Wave Frequencies. All the measurements described above were made at *microwave* frequencies between UHF (428 MHz) and K_a band (35 GHz). High-frequency (HF) radars usually operate in the frequency range between about 5 and 30 MHz, corresponding to wavelengths between 60 and 10 m, respectively. Since the operation of such radars takes place either by the ground wave or over ionospheric (*sky-wave*) paths spanning great ranges, the grazing angles tend to be small (between 0 and 20°). For these wavelengths and grazing angles, initial measurements by Crombie indicated that the scattering from the sea surface was the result of Bragg scatter from sea waves of one-half the radar wavelength.[4] In the years since these early measurements, there has been considerable activity in the field of HF radar and HF clutter,[43,44] and the results can be summarized as follows: For vertical polarization, the major energy of the HF clutter signal appears in spectral lines displaced to either side of the
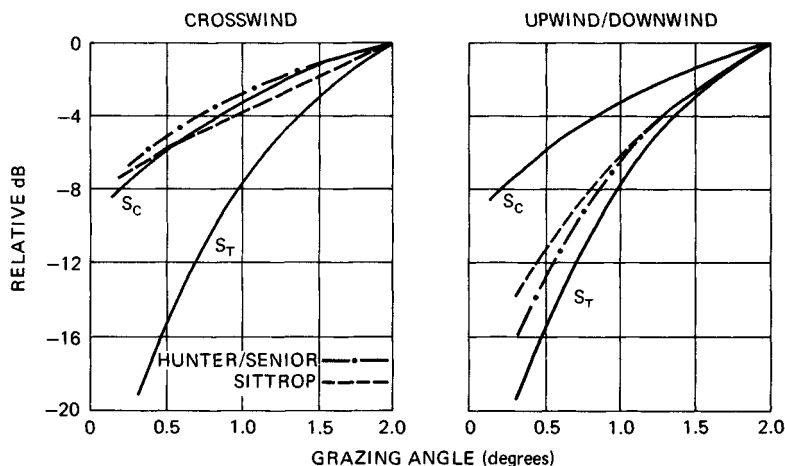
FIG. 13.13 Differential behavior of very low angle clutter for orthogonal wind directions: S_c is a conventional shadowing function;[41] S_T is a threshold-shadowing function.[38] *(Data from Hunter and Senior[39] and Sittrop.[40])*

carrier frequency by the frequency of sea waves having a wavelength equal to half the HF wavelength λ (in meters). The relative strengths of the plus and minus lines are determined by the proportion of advancing and receding Bragg-resonant wave components in the clutter cell. Provided the wind speed is greater than about $\sqrt{3\lambda}$ kn (with λ in meters) and the sea is fully developed, the clutter cross section σ^0 is about -27 dB and is relatively independent of wind speed and frequency. (The definition of σ^0 in HF radar is complicated by problems in properly defining antenna gains for ground-wave and sky-wave paths and by propagation effects due to the ionosphere.) The clutter spectrum tends to fill in around and between the lines as the wind picks up. For horizontal polarization (which is possible only over sky-wave paths), the cross section is much smaller and shows the characteristic fourth-power decay with decreasing grazing angle. For these HF wavelengths of tens of meters, the sea is relatively flat and the scattering laws are simple. A discussion of HF radar may be found in Chap. 24.

At the other end of the potentially useful radar spectrum, in the millimeter-wave band, the few published measurements of radar clutter lead to the conclusion that millimeter-wave backscatter behaves in much the same manner as backscatter at the lower microwave frequencies. This was suggested by the K-band curves shown in Fig. 13.5 for moderate wind speeds and further supported by some older shipboard data at frequencies between 9 and 49 GHz.[45] It should be noted that clutter signal paths lie close to the sea surface, where the atmospheric and water-vapor densities are highest. This means that at these higher frequencies the clutter signal will be strongly affected by the atmospheric absorption effects described in Chap. 2, and consequently the surface-related cross section inferred from the received signal strength in any given measurement will depend upon the path length. Moreover, the role of sea *spray* in both scattering and absorption will certainly be more important than at the lower microwave frequencies.

It is difficult to find clutter data at frequencies above K_a band, although H- and V-polarized returns at 95 GHz at a grazing angle of $1°$ were reported, both with values of close to -40 dB.[46,47] Interestingly, this is just the cross section

measured at this angle by a number of investigators at X band (see Ref. 12), showing a similarity between the returns at these two widely spaced frequencies. However, at lower frequencies, at L band and below, there is a noticeable tendency for the cross section to fall off with decreasing grazing angles below about 15 to 20°.

The Spectrum of Sea Clutter. The scattering features producing sea clutter are associated with a surface subject to several types of motion. The features may themselves be moving with small group or phase velocities over this surface while the surface, in turn, is moved by the orbital velocities of the larger waves passing across it. Or the scatterers might be detached from the underlying surface, as in the plumes emitted at the crests of breaking waves, and move at speeds much greater than the orbital speeds.[48] At higher radar frequencies and in strong winds, the possibility of scattering from spray, advected by the wind field above the surface, must be considered. All this complex motion shows up in a doppler shift imparted to the scattered electromagnetic wave.

Surprisingly few measurements of microwave clutter spectra for real seas have been reported in the literature, and those few that exist can be separated into aircraft measurements of the spectral shape alone[49,50] and fixed-site shore measurements showing a shift in the spectral peak.[51,52] All these studies were performed at relatively low grazing angles (less than 10°), although Valenzuela and Laing include a few measurements up to 30°. Other measurements of sea clutter spectra include those made at much lower frequencies in the HF band, as described in the last section, those made under artificial conditions in the wave tanks,[53] whose application to real-sea conditions is uncertain, and other fixed-site measurements at high resolution and short averaging times, to be discussed later.

As it turns out, microwave sea clutter spectra have a rather simple form at the lower grazing angles. Figure 13.14 illustrates typical spectral behavior at the two polarizations, based on data collected by Pidgeon for C-band clutter looking upwind at a few degrees grazing.[51] The peak frequency of the upwind spectrum appears to be determined by the orbital velocity of the largest sea waves, plus a wind-dependent velocity increment containing, but not entirely explained by, wind-induced surface currents. The orbital velocity V_{orb} is taken to be that of the major waves and is obtained in terms of significant height $H_{1/3}$ and period "T" from the expression

$$V_{orb} = \pi H_{1/3} / \text{``}T\text{''} = 0.1U \qquad (13.10)$$

The approximate dependence on wind speed U was found by substituting $H_{1/3} = 3h_{rms}$ from Eq. (13.6), assuming a *fully developed sea*, and T from Eq. (13.5). To this there must be added a wind-drift velocity of about 3 percent of U and a fixed *scatterer* velocity (which appears to be about 0.25 m/s in the X- and C-band measurements[51,52,54]). Summing these components yields the virtual doppler velocity at the peak of the clutter spectrum for the particular case of a *vertically polarized, X- or C-band* radar looking *upwind* at *low grazing angles*:

$$V_{vir} \approx 0.25 + 0.13U \qquad \text{m/s} \qquad (13.11)$$

(As noted earlier, care must be taken whenever wind speed is used to parameterize a process that depends on waveheight. There is an unambiguous relation only for a fully developed sea in the absence of swell.) The remaining properties

of the clutter spectrum can now be discussed in terms of V_{vir}. For example, the spectral peak for *horizontal* polarization follows a similar linear dependence on U, only with a coefficient lying somewhere between 0.17 and 0.20, as reflected by the sketch in Fig. 13.14. The (half-power) width of the clutter spectrum is roughly the same for both polarizations and is equal approximately to the upwind vertical velocity given in Eq. (13.11). For look directions away from upwind, the peak doppler follows a cosine dependence very closely, going to zero at crosswind aspects and turning negative downwind. Interestingly, the *bandwidth* of the spectrum remains relatively constant.
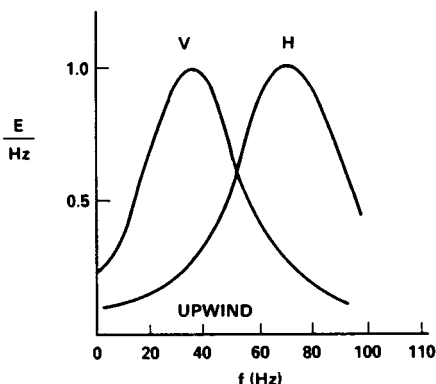

FIG. 13.14 Qualitative behavior of doppler spectra of sea clutter looking upwind at low grazing angles. (*Based on C-band measurements by Pidgeon.*[51])

The details of the clutter spectrum show little dependence on either the radar frequency or the grazing angle, at least for angles less than about 10°. In reviewing the results of measurements at four frequencies—UHF, L, C, and X bands—Valenzuela and Laing[50] noted a relatively weak tendency of clutter bandwidth to decrease with increases in frequency between the UHF and X bands and grazing angles between 5 and 30°. Since both of these variations entail a decrease in the size of the radar footprint on the surface, they might be due to a dependence on resolution cell dimensions, although the other workers found that the pulse length had little effect on clutter bandwidth for values between about 0.25 and 10 μs. The equivalence between time and space averaging in sea clutter measurements was discussed earlier, and in the case of clutter spectra the averaging times were all quite long (of the order of 10 to 20 min), which should be sufficient to stabilize the spectra for almost any resolution cell size.

Spectra obtained with *short* averaging times disclose something of the origins of the clutter spectrum. Figure 13.15 is a sequence of 0.2-s spectra obtained by Keller et al.[55] with a coherent vertically polarized X-band radar operating at a grazing angle of 35° and a resolution cell size of about 10 m². The zero-doppler reference in this figure was located arbitrarily at −16 Hz, and because of the high grazing angle the effects of both senses of the orbital velocities are seen, unlike the low-angle shadowed surface results shown in Fig. 13.14. The spread along each line is due to the small-scale wave motions on the surface, while the larger meanders are induced by the orbital velocities of the large waves moving

through the measurement cell. The wind speed was 16.5 m/s, and a doppler shift of 100 Hz corresponds to a radial velocity of 1.6 m/s. The average clutter spectrum expected for this wind speed and grazing angle, with bandwidth obtained from Eq. (13.11), is sketched on the figure. The large spectral spike appearing in the center of the display is no doubt due to a wave breaking in or close to the measurement cell. The doppler velocity for this spike suggests a peak scatterer velocity of about half the wind speed, which would correspond to the group velocity of the longest waves on the surface. Although such events are relatively rare in a fixed area of 10 m², they should occur quite frequently within a large surveillance cell and might often have large scattering cross sections associated with them.
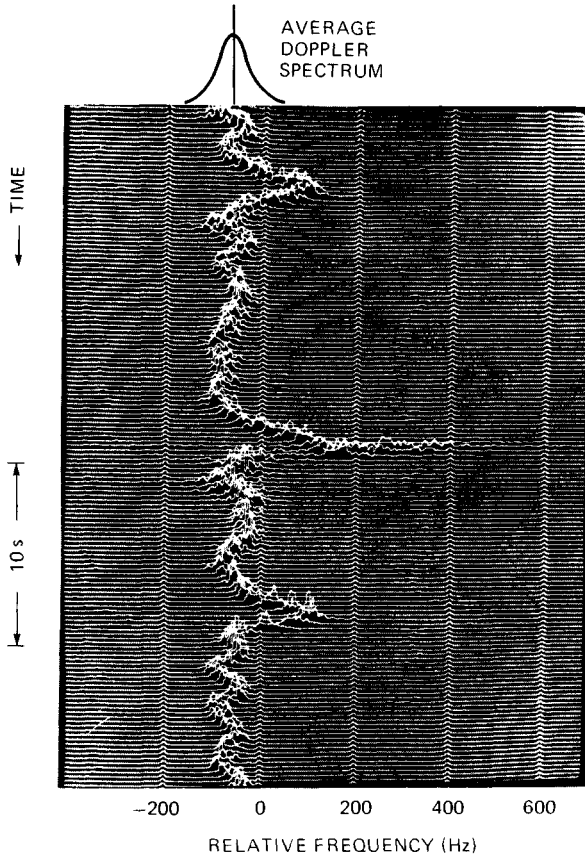

FIG. 13.15   Short-time averaged doppler spectra at X band for an intermediate grazing angle of 35°; spectra computed at 0.2-s intervals. (*From Keller et al.*[55])

Other Effects on Sea Clutter

Rain.   Evidence of the effect of rain on sea clutter is mainly anecdotal; for example, radar operators report that sea clutter tends to decrease when it starts to rain. However, there has been little in the way of reliable, quantitative experi-

mental information about the interaction between rain and wind-driven sea scatter. Laboratory measurements by Moore et al.[56] with artificial "rain" suggested that for light winds the backscatter level increased with the rain rate, while for heavy winds rain made little difference. In measurements in natural rain over Chesapeake Bay, Hansen[57] found that even a light rain (2 mm/h) changes the spectral character of sea clutter at moderate wind speeds (6 m/s) by introducing a significant high-frequency component. He also found some evidence in support of the radar operators, at least for the low grazing angles and horizontal polarizations with which most shipboard radars operate. Figure 13.16 compares the correlation function of sea clutter (X band, low grazing angle, H polarization) with and without rain for a 15-kn wind speed and a rain rate of 4 mm/h. The sharp decrease in correlation time in the presence of rain reflects the broadening of the clutter spectrum. Beyond this, there is virtually no quantitative information about the effect of rain on existing sea clutter.
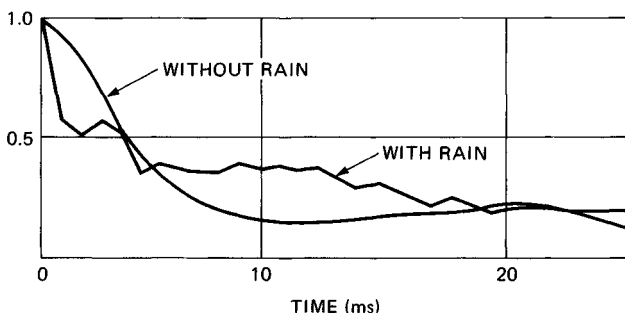

FIG. 13.16 Effect of rain on the correlation function of wind-driven sea clutter; X band, horizontal polarization, wind speed 15 kn, rain rate 4 mm/h. (*From Hansen.*[57])

The production of sea clutter by rain falling on a "calm" surface in the absence of wind was also investigated by Hansen, with the results shown in Fig. 13.17.[57] A high-resolution X-band radar (40-ns pulse, 1° beamwidth), operating at a grazing angle of about 3°, viewed the backscatter from a fixed spot on the windless surface of Chesapeake Bay as the rain steadily increased from 0 to 6 mm/h. The cross sections for vertical and horizontal polarizations were quite different for low rain rates but tended to merge at a rain rate of about 6 mm/h. The magnitude of this *splash* cross section rose to a σ^0 of about −40 dB, corresponding to wind-induced cross sections at this grazing angle for winds of about 10 kn. Further laboratory[58] and theoretical[59] studies have shown that the major scattering feature is the vertical *stalk* that emerges shortly after drop impact. Moreover, these studies suggest that the V-polarized returns from raindrop splashes should be relatively insensitive to the rain rate, while the H-polarized returns should show a strong dependence on both the rain rate and the drop-size distribution.

Propagation Effects. Another topic in sea clutter that has been largely unexplored is the role played by *propagation effects* within the atmospheric boundary layer lying over the sea surface. The effects of atmospheric absorption have been noted above in connection with millimeter-wave clutter. However, at very low grazing angles the ray paths joining the radar to the surface become very sensi-
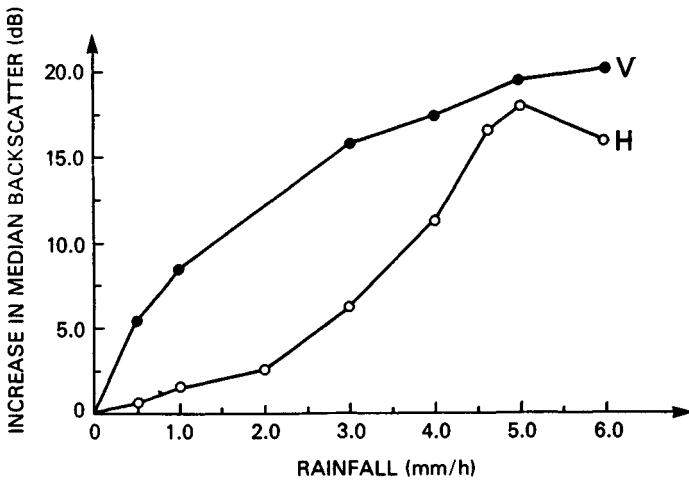
FIG. 13.17 Sea clutter produced by rain splashes alone on a calm surface. (*From Hansen.*[57])

tive to refractive inhomogeneities in the atmospheric boundary layer. Over distances approaching and beyond the conventional optical horizon, such perturbations could produce strong focus-defocus variations along the illumination profile[60] or a general rise in the local grazing angle.[38] Figure 13.18 gives an experimental example of the effect of *ducting* on very low angle sea clutter.[42] Since the grazing angle given as the abscissa is actually a plot of inverse range, the lifting of the cross section by ducting over an order-of-magnitude span of ranges is very likely due to a rise in the mean grazing angle produced by refraction in the evaporative layer.[38] Such effects should be suspected whenever the radar propagation path extends beyond the *optical* horizon.
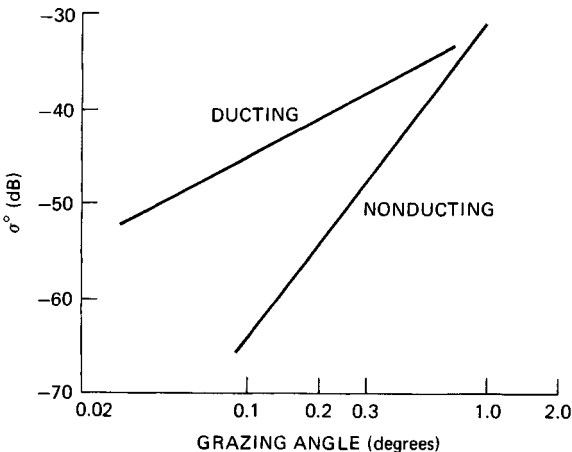

FIG. 13.18 Effect of ducting on low-angle clutter; wind speed about 10 kn.

Shadowing.   The possibility of shadowing must be seriously considered whenever the sea is viewed at grazing angles smaller than the rms slope angle of the sea surface. Some examples were discussed earlier in connection with the behavior of sea clutter at low grazing angles in Fig. 13.13. In fact, the sharp falloff of the *nonducting* data in Fig. 13.18 gives further evidence of the *threshold shadowing* mentioned there. However, the common idea of shadowing, along with all existing theories of a shadowed surface, rests on the geometrical optics concept of a sharp transition between light and darkness. By considering the implications of diffraction at the wave peaks, it is possible to determine the domain of radar frequencies and wind speeds over which the concepts of geometrical optics may be applied. This was done by Wetzel,[12] who showed in detail how diffraction, rather than shadowing, controls propagation into and out of the troughs of the waves under many of the usual frequencies and wind speeds encountered in practical radar operations at low grazing angles. For example, shadowing will take place at K_a band for any winds above 15 kn, yet will hardly ever occur at L-band frequencies.

Contaminants.   The idea of pouring oil on troubled waters is a familiar one: the angry surface will smooth and subside. In another age, the survival-gear locker of every sailing ship would contain a bottle of oil to quiet the sea in a storm. Although the effectiveness of this procedure has always been somewhat controversial, there is no question that oil can produce a *slick* of smooth water at relatively low wind speeds. In fact, biological oils, produced by bacteria, algae, and plankton, can be found everywhere on the world's oceans and form natural slicks in those regions that combine the greatest oil concentration with the lowest wind speeds, e.g., close to continental shorelines.[61] Human-made contaminants can, of course, have the same effect. A layer of oil only 1 molecule thick will significantly affect the ability of the surface to support wave motions, but this layer must be continuous. The adjacent molecules then sense each other and form a film that is resistant to horizontal compression. The surface elasticity is changed, a type of longitudinal viscosity is introduced, and the surface becomes stabilized against the growth of short waves up to several inches in length.[62,63]

To the extent that radar sea clutter is produced by small-scale surface roughness (at grazing angles less than about 80°), the presence of oil on the surface should lead to a measurable decrease in clutter cross section. But, as noted above, the reduction of small wave motions requires the existence of a *continuous* monolayer; slick formation is a go–no-go process, and so slicks will tend to have relatively sharp boundaries. In operating the NRL 4FR system as a synthetic aperture radar to obtain images of the slicks produced by oil spills, Guinard found that the slicks were well defined, that it took very little oil to maintain a visible slick, that vertical polarization provided much greater contrast than did horizontal, and that the slicks were quenched by winds and currents.[64] Although signal strength was not recorded in this imaging experiment, later measurements at X and L bands by others[65] indicated that at the higher grazing angles (about 45°) the clutter reduction produced by the types of oil occurring in *natural* slicks was rather small, of the order of a few tenths of a percent. Since slicks are dispersed by the wind and associated wave action at wind speeds greater than about 10 kn, the effect of natural slicks on clutter may not be clear because they tend to occur in the regime of low wind speeds where the sea surface is already ill defined.

The celebrated *sun glitter* measurements by Cox and Munk[66] gave a quantitative measure of the effect of contaminants on the surface slopes in open water, showing that the wind-generated component of the rms slope of "oiled" waters is significantly smaller than that of "clean" water. The heavy human-made oils used in their experiment were effective in suppressing small-scale waves over a range of wind

speeds well beyond those which would normally disperse the lighter natural oils; so the effect of oil spills on sea clutter should be expected to extend to the higher wind speeds. In fact, at these higher wind speeds the depression of radar backscatter by such oils at X and K_a bands can reach 10 to 20 dB at intermediate grazing angles between 30 and 60°.[67,68]

Currents. The most obvious effect of a current on sea clutter would be a shift in the peak of the doppler spectrum, similar to the contribution of the 3 percent wind-drift current mentioned in connection with Eq. (13.8). Another effect is related to the fact that the excitation of the surface-wave system depends on the *apparent* wind; so there can be significant differences in waveheight according as the wind is blowing with or against the current. According to Eq. (13.6), waveheight is proportional to the square of the wind speed; so in the Gulf Stream, for example, with a current of 4 kn flowing north, a 15-kn northerly blowing against the current will raise a sea 3 times as high as a 15-kn southerly blowing with the current. Even with no wind the presence of strong current shears can produce highly agitated surfaces. Shipboard observers have reported bands of roaring breakers passing by on an otherwise-smooth surface, presumably produced by powerful surface-current shears associated with large-amplitude internal waves.[69] In a more subtle way, currents are held responsible for synthetic aperture radar (SAR) images which contain the expression of bottom topography in shallow waters.[70] In each of the examples cited above, the current produces a change in the surface roughness, which can be expected to give rise to a change in sea clutter cross section.

Combined Effects. Some idea of the complexity within a clutter scene due to *other effects* may be obtained from Fig. 13.19, which shows a digitized PPI display of clutter in the Sargasso Sea, under light wind conditions and near a thermal oceanic front.[71] Although all possible contributing effects were not identified, observers noted the presence of human-made detritus organized by the currents at the edges of the thermal front, slicks probably of both natural and artificial origin, fronds of seaweed close to the surface, and the presence of light and variable winds. The dynamic range of the digitized (false-color) PPI was 30 dB, and some of the clutter contrasts, across what are obviously extremely sharp boundaries, were almost this great.

13.4 THEORIES OF SEA CLUTTER

The sea surface is so rich in potential scattering structures that in seeking to understand the phenomenology experimenters and theorists alike have proposed and have found support for almost any imaginable model. However, aside from providing an intellectual basis for "understanding" sea clutter phenomena, a theory of sea clutter should serve the practical purpose of providing accurate a priori predictions of all aspects of clutter behavior under all possible environmental conditions. At present, the theory of sea clutter does neither of these tasks very well and must be thought of as a book with the final chapters still to be written.

Before discussing the current theories of sea clutter, it is important to distinguish them from other so-called sea clutter models that are designed to provide a predictive capability. Some such models organize large quantities of empirical data by finding a multiple linear-regression formula relating the clutter cross section to a variety of parameters, such as grazing angle, wind speed, frequency, etc., all measured concurrently.[1,40] Even a multiparameter matrix tabulation